Generation of Monolayer Gradients in Surface Energy and Surface Chemistry for Block Copolymer Thin Film Studies

Julie N. L. Albert,[†] Michael J. Baney,[†] Christopher M. Stafford,[‡] Jennifer Y. Kelly,[†,‡] and Thomas H. Epps III[†,*]

[†]Department of Chemical Engineering, University of Delaware, Newark, Delaware 19716, and [‡]Polymers Division, National Institute of Standards and Technology, Gaithersburg, Maryland 20899

ABSTRACT We utilize a vapor deposition setup and cross-diffusion of functionalized chlorosilanes under dynamic vacuum to generate a nearly linear gradient in surface energy and composition on a silicon substrate. The gradient can be tuned by manipulating chlorosilane reservoir sizes and positions, and the gradient profile is independent of time as long as maximum coverage of the substrate is achieved. Our method is readily amenable to the creation of gradients on other substrate surfaces, due to the use of vapor deposition, and with other functionalities, due to our use of functionalized chlorosilanes. Our gradients were characterized using contact angle measurements and X-ray photoelectron spectroscopy. From these measurements, we were able to correlate composition, contact angle, and surface energy. We generated a nearly linear gradient with a range in mole fraction of one component from 0.15 to 0.85 (34 to 40 mJ/m^2 in surface energy) to demonstrate its utility in a block copolymer thin film morphology study. Examination of the copolymer thin film surface morphology with optical and atomic force microscopy revealed the expected morphological transitions across the gradient.

KEYWORDS: surface energy · surface chemistry · monolayer · gradient morphology · block copolymer · thin film

Surface energy and surface chemistry play an important role in a number of chemical and biological processes including adhesion,[1,2] surface wettability,[1,3,4] molecular self-assembly,[1,5−8] protein adsorption,[1,9] and cell attachment, growth, and proliferation.[1] Understanding the role of surface energy/chemistry in these processes is therefore vital to engineering surface coatings, fabricating templates from self-assembling materials, and mimicking biological interfaces. Such applications require that a large parameter space of surface energies and chemistries be explored, making combinatorial and/or high-throughput approaches desirable. Gradients in surface energy/chemistry enable high-throughput studies because a continuous range of surface energies/chemistries can be explored on a single surface, enabling faster screening and discovery of materials and phenomena. Additionally, surface energy/chemistry gradients have been used to drive the motion of water droplets on a surface,[10] to probe polymerization kinetics,[1] to direct the movement of dendritic macromolecules on surfaces,[11] and to study cell migration.[1]

A number of methods exist for generating surface energy gradients, each having benefits and drawbacks. As a result, the method selected often depends on the intended application.[1] The most common chemistries employed in gradient formation involve the attachment of organosilanes to silica or thiols to gold, with silica being more commonly used in applications requiring high thermal stability and gold more commonly used in biological applications. We briefly discuss some of the major work in this area to illustrate the principles underlying surface energy and surface chemistry gradient formation.

A single-component gradient typically relies on the creation of a gradient in surface coverage. For example, a hydrophobic component can be deposited on a hydrophilic substrate. Elwing *et al.* introduced a liquid deposition technique to generate such a gradient for protein adsorption studies.[9] Chaudhury and Whitesides modified this technique, using vapor deposition to generate a gradient for driving the motion of water droplets.[10] Their method has since been used by others to generate gradients for controlling the motion of liquid drops on surfaces[12,13] and manipulating the grafting densities of polymer brushes and nanoparticles.[1,14] Choi and Newby employed contact printing, which utilizes a dilute solution of the material to be printed and an elastomeric stamp, to produce a single-component gradient on a micrometer length scale.[15] Kraus *et al.* expanded on this idea, using mass transfer theory to

*Address correspondence to thepps@udel.edu.

Received for review July 6, 2009 and accepted November 16, 2009.

Published online December 1, 2009.
10.1021/nn900750w

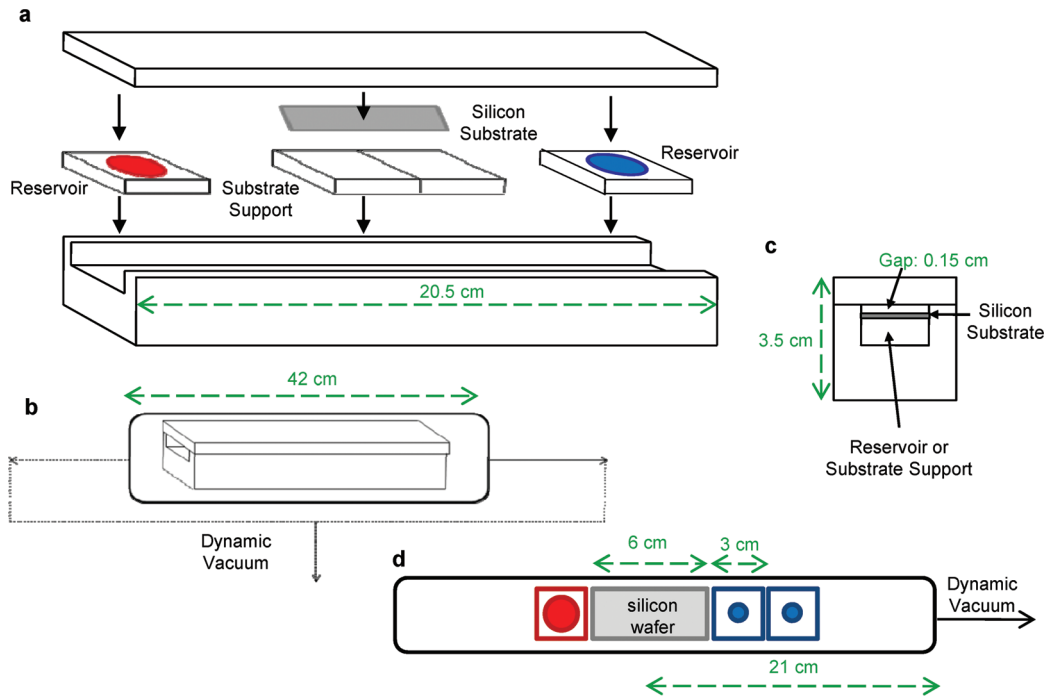

Figure 1. Device schematic. (a) Reservoirs and substrate are loaded into the Teflon insert. (b) Insert is loaded into the deposition chamber. The deposition occurs under dynamic vacuum. Vacuum connections can be made at one or both sides of the chamber. (c) Gap between the substrate and the insert cover is small compared to the length of the insert, as illustrated in this cross-sectional view. (d) Schematic representation of setup used to generate the gradient discussed in this work.

design stamps for generating gradients of different shapes and steepness on longer length scales.[16]

To generate two-component gradients, these single-component methods can be extended by backfilling with a second component after the initial deposition.[16,17] Replacement lithography, in which molecules of an initial monolayer are desorbed from the surface in a gradient fashion and the resulting empty sites backfilled with a second component, has been demonstrated with thiols on gold.[1] Alternatively, a single-component monolayer can be modified to introduce additional functionality. Graded ultraviolet/ozone (UVO) treatment of a hydrophobic monolayer has been used to generate a gradient in hydrophilicity, with the density of oxidized chain ends along the gradient being proportional to the radiation exposure time.[18] This technique has been used to study dewetting behavior of thin polymer films,[4] to examine the effect of surface energy on block copolymer phase behavior,[5] and to introduce alkyne functionalities suitable for "click chemistry" attachment of biologically relevant molecules.[19]

TABLE 1. Static Contact Angle Measurements of Pure Component Monolayers[a]

contact angle liquid	benzyl silane monolayer	methacryl silane monolayer
diiodomethane	40.9 ± 0.5°	53.5 ± 0.5°
ethylene glycol	52.3 ± 0.8°	59.6 ± 1.8°
water	78.4 ± 1.1°	82.6 ± 1.7°

[a]The uncertainty represents one standard deviation of the data from repeated measurements, which is taken as the experimental uncertainty of the measurement.

Hydrolysis and X-ray-induced chemical modification have been used to produce chemical changes in monolayers on gold, but these techniques have not yet been employed in a gradient fashion.[20,21]

Finally, a number of researchers have used polymer or copolymer brushes to create surface energy gradients for block copolymer thin film studies. These gradients can be generated by grafting or synthesizing two types of polymers on a surface in a gradient fashion or by synthesizing statistical copolymers on the surface with a gradient in composition.[1] The latter method requires manipulation of the monomer composition above the substrate surface either by adding or by removing a monomer during synthesis[1] or by microfluidic mixing of two monomers to generate a gradient in monomer composition above the substrate prior to initiation.[22] More recently, Elkasabi and Lahann used a chemical vapor deposition polymerization in which they cross-diffused monomers to the substrate surface for reaction.[23]

Unfortunately, the above methods either provide limited gradient tunability or involve complex processes that are not easily adapted to new systems. The liquid and vapor deposition techniques, as applied in the literature, result in time-dependent and sigmoidal gradient profiles that are not easily tuned.[14] Furthermore, liquid deposition imposes an additional requirement of compatibility between the substrate and deposition solvent. Contact printing affords gradient tunability but requires understanding of mass transfer to design suitable stamps and chemical compatibility

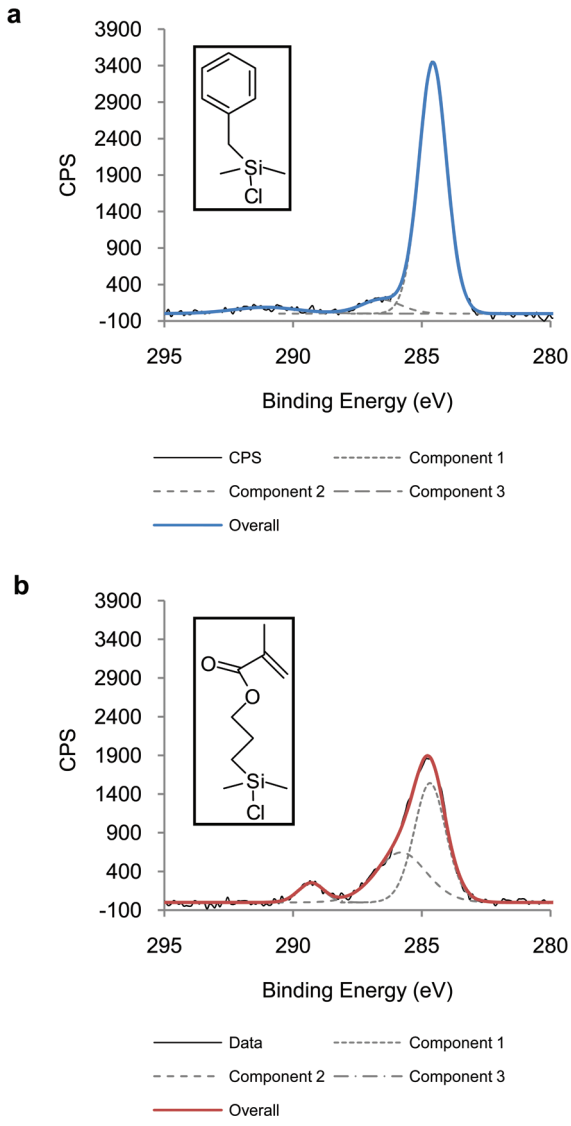

Figure 2. Peak-fitting of high-resolution XPS C 1s spectra for (a) pure benzyl silane monolayer and (b) pure methacryl silane monolayer. Insets in each figure show the structure of the chlorosilane used to fabricate each monolayer.

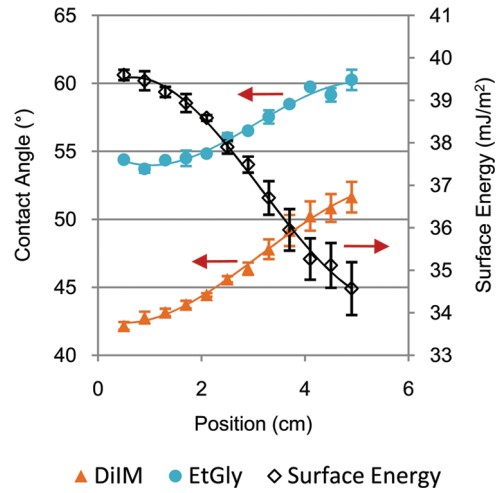

Figure 3. Contact angle and surface energy characterization of the gradient. Solid lines (—) indicate the data trend lines. However, linear fits (not shown) to the diiodomethane contact angle and surface energy data through the region of interest also capture the trends well despite the slight curvature in both sets of data. The error bars represent one standard deviation of the data from repeated measurements, which is taken as the experimental uncertainty of the measurement.

between the ink pad, the stamp, and the printing surface. Replacement lithography is a time-consuming process and, due to the desorption step, has been applied to thiol monolayers on gold but is not amenable to surface reaction chemistries such as organosilanes on silica. For many applications requiring processing at elevated temperatures (*e.g.*, thermal annealing of polymer films), thiol chemistry is undesirable because the thiol molecules diffuse on the substrate surface[24] or desorb at relatively low temperature (≈70 °C in air),[25] and the fabricated gradient would be lost during processing. The UVO treatment method enables formation of linear gradients, but the oxidation process limits the range of surface chemistries that can be created; some functionalities (*e.g.*, halogen, amine) could not be formed by this process. Furthermore, these gradients are susceptible to degradation, having a shelf life of only a few days under atmospheric conditions or a few weeks when stored in a cool, dark desiccator.[26] Finally, polymer brush approaches require an understanding of polymer synthesis techniques and the associated complex kinetic processes in order to achieve the desired result.

In the present work, we present a controlled vapor deposition method for the facile generation of two-component gradients, overcoming some of the limitations and difficulties associated with current methods. We demonstrate the utility of this method by generating a linear gradient and using it to examine the phase behavior of a cylinder-forming poly(styrene-*b*-methyl methacrylate) (PS-*b*-PMMA) thin film, locating the expected morphological changes along the gradient.

RESULTS AND DISCUSSION

The gradients were created by vapor deposition of functionalized chlorosilanes onto UVO-cleaned silicon substrates under dynamic vacuum. The use of dynamic vacuum establishes directional flow within the deposition chamber throughout the duration of the deposition process. Because we utilized vapor deposition, the need for compatibility between the substrate and a deposition solvent was eliminated, making the technique amenable to a variety of substrate surfaces, including, potentially, polymer surfaces, which are often incompatible with common organic deposition solvents (*e.g.*, toluene). The use of functionalized chlorosilanes afforded tunability in surface chemistry, or surface functionality, as well as surface energy range. For example, gradients could be created with a relatively narrow surface energy range (≈6 mJ/m^2 in this work) for high-resolution examination of morphology changes in polymer films, or gradients with a larger surface en-

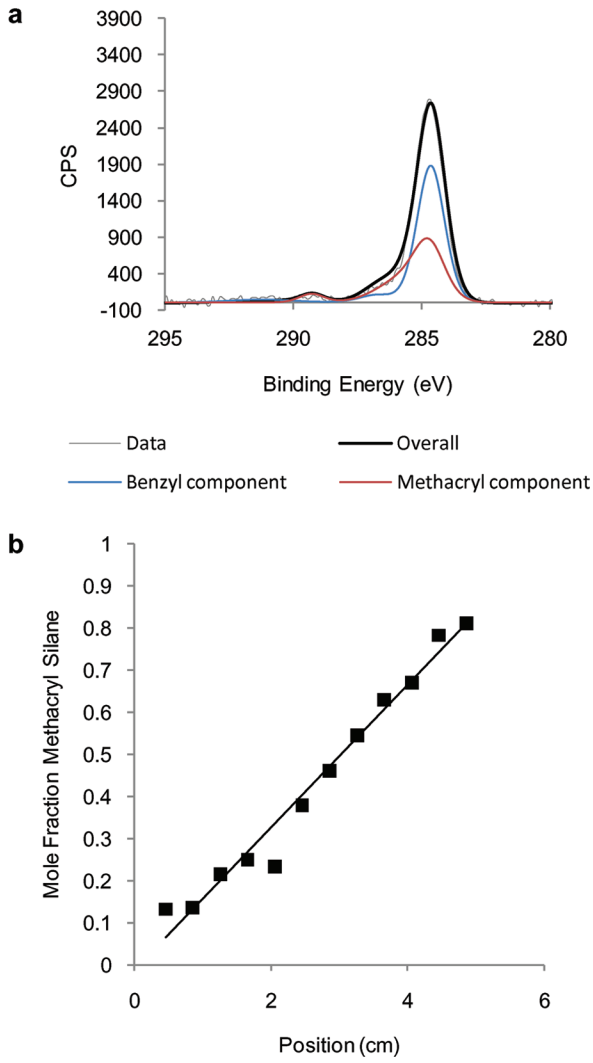

Figure 4. (a) Curve fitting of a gradient point as a linear combination of the pure monolayer C 1s spectra. The mole fraction of methacryl silane at this location was 0.54. (b) Composition characterization of the complete gradient from XPS data with linear fit shown. Each data point represents a single measurement along the gradient.

ergy range could be created for a broader survey, simply by changing the chlorosilane functionalities. Cross-diffusion of the chlorosilanes resulted in a single-step deposition process. Our device permits control of the chlorosilane deposition profiles by manipulating chlorosilane reservoir size and placement based on the relative vapor pressures of the components and the desired gradient profile. We confined diffusion to a small gap (≈1.5 mm) above the substrate surface. The degree of confinement also affects the chlorosilane deposition profiles, making it another parameter that could be used to tune the gradient profile. Additionally, the characteristics of the gradient were independent of time as long as maximum coverage of the surface was achieved. The gradients were characterized with static contact angle measurements and X-ray photoelectron spectroscopy (XPS). We demonstrated the utility of this device by generating a linear gradient and using it to examine the phase behavior of a cylinder-forming PS-*b*-PMMA thin film. The orientation of the block copolymer thin film morphology (parallel or perpendicular relative to the substrate surface) is known to depend on the substrate surface energy.[2] We located the expected morphological changes along the gradient, thereby validating the utility of our gradients. Furthermore, our polymer-coated gradient behavior is amenable to high-throughput thin film specimen preparation techniques recently developed by Roskov *et al.* and references therein.[27]

Device Used to Generate Gradient Monolayers. The device used in gradient fabrication consists of a Teflon insert and a vacuum chamber, as depicted schematically in Figure 1. The Teflon chlorosilane reservoirs and substrate are loaded into the Teflon insert (Figure 1a), which is then placed inside the vacuum chamber (Figure 1b). The insert serves to confine vapor diffusion to a small gap (≈1.5 mm) above the substrate surface (Figure 1c). The vacuum chamber contains ports on either side such that vacuum can be pulled from one or both ends, symmetrically or asymmetrically (Figure 1b); the ports also could be used to fill the chamber with an inert gas for deposition. The gradient profile is most easily tuned by adjusting the size and positions of the reservoirs. The specific setup used to generate the linear gradient presented in this work consisted of two 1/4′′ (6.35 mm) diameter reservoirs of benzyldimethylchlorosilane (benzyl silane) and one 1/2′′ (12.7 mm) diameter reservoir of 3-methacryloxypropyldimethylchlorosilane (methacryl silane), placed on either side of the substrate, with the benzyl silane reservoirs closest to the vacuum outlet (Figure 1d). These chlorosilane functionalities were specifically chosen to mimic the molecular structure of PS-*b*-PMMA, with the benzyl silane being chemically similar to the PS block and the methacryl silane similar to the PMMA block.

Pure Component Monolayer Characterization. Pure component monolayers were generated with the same setup described above, except that all reservoirs were filled with a single component, either benzyl silane or methacryl silane. The static contact angle characterization of these monolayers with water, diiodomethane, and ethylene glycol is given in Table 1. The two monolayers were easily distinguished by diiodomethane and ethylene glycol contact angles; however, the water contact angles were too close in value to be useful for gradient characterization. The surface energies calculated from the diiodomethane and ethylene glycol contact angles were 40.4 mJ/m^2 for the benzyl silane and 33.9 mJ/m^2 for the methacryl silane.

The pure component monolayers were further characterized with XPS and were distinguishable by their carbon 1s (C 1s) spectra, due to the carbon−oxygen binding signal in the methacryl silane structure, as shown in Figure 2. We fit the major components of these spectra to generate the overall envelope of each curve for later use in our gradient analysis. Survey spec-

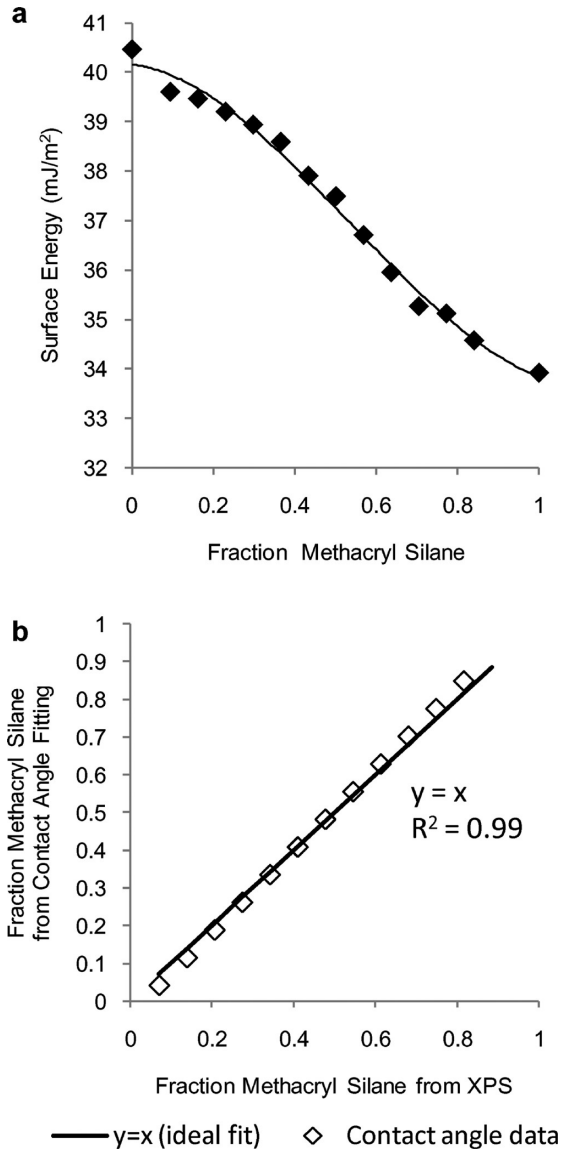

Figure 5. (a) Correlation between surface energy and composition. (b) Comparison of composition determined from diiodomethane contact angle with composition determined by XPS for each data point along the gradient. The comparison follows the expected $y = x$ trend line, validating the use of diiodomethane contact angle as an estimator of composition for the two-component system studied.

tra and high-resolution oxygen 1s (O 1s) and silicon 2p (Si 2p) spectra also were acquired; these spectra are provided in the Supporting Information (Figure S1). Only the expected peaks from oxygen, carbon, and silicon were located on the survey spectra. Both O 1s spectra showed a single peak indicating that the carbon−oxygen binding in the methacryl silane was not distinguishable from the silicon−oxygen binding in the native oxide layer of the silicon substrate. Likewise, the Si 2p spectra showed only the peaks for the oxide and crystalline silicon.

Gradient Monolayer Characterization. The gradient was initially characterized using static contact angle measurements with diiodomethane and ethylene glycol as probe fluids, and the corresponding surface energies were calculated using a geometric mean combining rule proposed by Owens and Wendt[28] (details in Methods). These results are shown in Figure 3. A linear fit (not shown) to the diiodomethane (DiIM) contact angle data captures the trend well ($r^2 \approx 0.98$), despite the slight curvature in the data. The ethylene glycol (EtGly) contact angle clearly has a nonlinear profile. However, both sets of contact angle measurements indicate that the gradient is primarily benzyl silane at the beginning (position ≈0 cm, with diiodomethane and ethylene glycol contact angles close to 41 and 53°, respectively) and primarily methacryl silane at the end (position ≈6 cm, with diiodomethane and ethylene glycol contact angles close to 53 and 61°, respectively). The surface energy decreases nearly linearly across the substrate from the benzyl silane end to the methacryl silane end, as expected since PS has a slightly higher surface energy (≈43 mJ/m^2) than PMMA (≈41 mJ/m^2).[29]

The composition of the gradient also was characterized with XPS. Multiple locations along the gradient were sampled, and the C 1s spectrum from each location was fit as a linear combination of the pure benzyl silane and pure methacryl silane monolayer spectra, as shown in Figure 4a. The composition at each location was estimated from the relative contributions of each curve to the overall fit. All gradient C 1s spectra, fits, and associated errors are provided in the Supporting Information (Figure S2). Figure 4b shows the change in composition, given by mole fraction of methacryl silane, across the gradient. In agreement with contact angle measurements, the gradient is primarily benzyl silane at the beginning and methacryl silane at the end, with the composition changing linearly in between those two locations. The positions of the data points were shifted −4.4 mm to account for differences in setting of the "zero" positions during XPS and contact angle data collection. The first XPS data point was excluded in fitting the linear trend line because it was outside the range of positions for which contact angle data were collected.

Thus, the contact angle/surface energy and XPS/composition characterization of the substrate surface indicate that the gradient generated with our controlled vapor deposition method is linear. If we examine the sigmoidal profile observed in the implementation of traditional diffusion-based gradient methods, we note that the middle portion of this profile is nearly linear. We believe that the geometric constraints and dynamic vacuum applied in our method result in directed deposition that enables us to capture the linear portion of the traditional concentration profile. Additionally, we can adjust the geometry (*e.g.*, reservoir sizes and positions) to manipulate the steepness of the linear profile and produce a gradient that is primarily benzyl silane at one end of the substrate and methacryl silane at the other end.

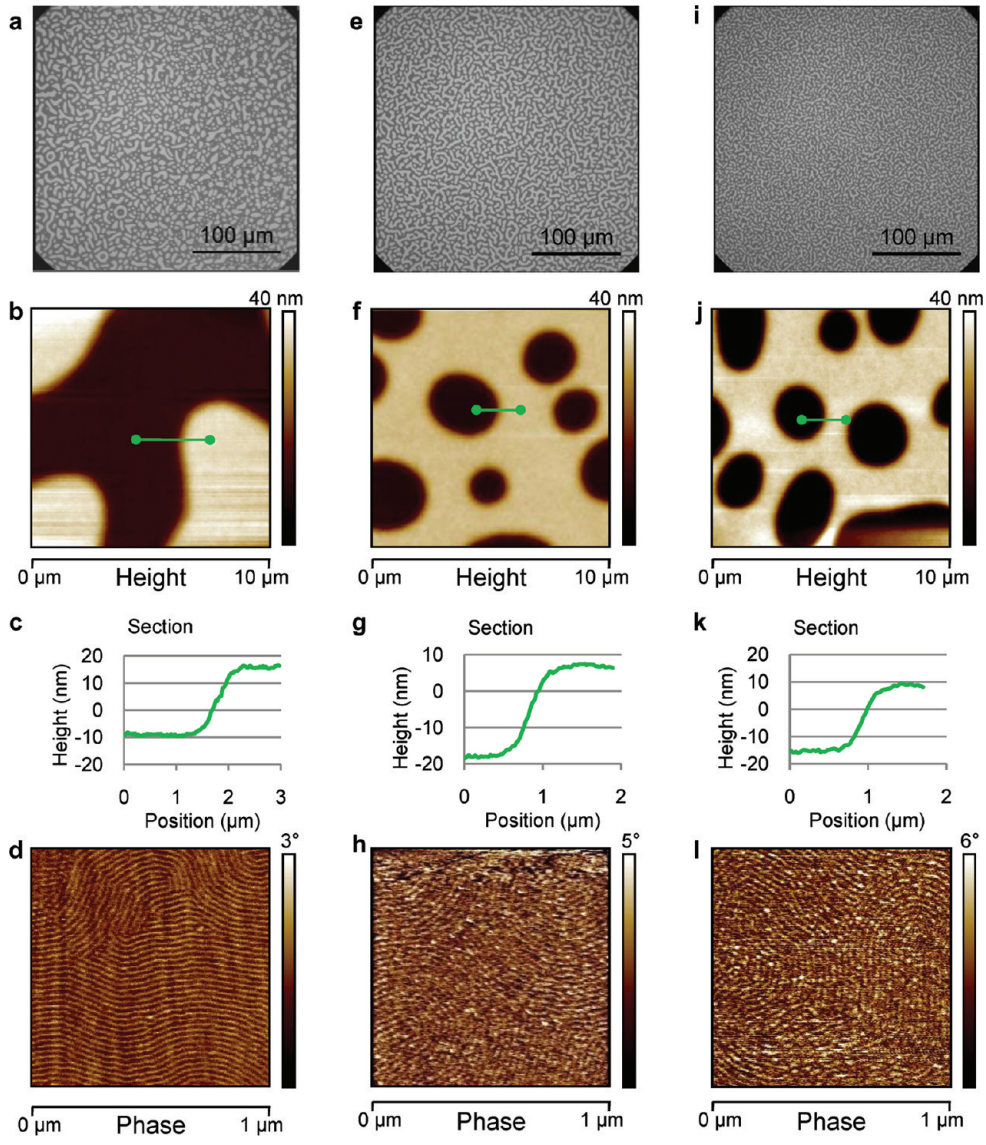

Figure 6. Optical and atomic force microscopy of PS-*b*-PMMA films on silicon (a−d), benzyl silane monolayer (e−h), and methacryl silane monolayer (i−l). Optical micrographs (a,e,i) show island/hole features. AFM height images (b,f,j) and corresponding sections (c,g,k) show that the difference between the high and low regions is ≈24 nm, or 1 × L_0, confirming that these are island/hole structures. AFM phase images (d,h,l) reveal parallel microstructure on all of these films. The diiodomethane (DiIM), ethylene glycol (EtGly) and water contact angles, and the surface energy (γ_s) of each surface are provided for reference.

With these results, we correlate surface energy with composition and find the nearly linear ($r^2 \approx 0.98$) relationship shown in Figure 5a. This correlation enables us to target desirable surface energies by manipulating monolayer composition or, conversely, to deduce the surface energy for a targeted monolayer composition.

Furthermore, as both diiodomethane contact angle and composition are nearly linear functions of position (Figure 3 and Figure 4b), composition can be inferred from contact angle measurements by interpolating between the pure component monolayer values according to the following equation: $x_m = (\theta - \theta_b)/(\theta_m - \theta_b)$, where x_m is the mole fraction of methacryl silane, θ is the diiodomethane contact angle at a gradient point or of a mixed monolayer, and θ_b and θ_m are the contact angles of the pure benzyl silane and pure methacryl silane monolayers, respectively. The compositions calculated from diiodomethane contact angles using the

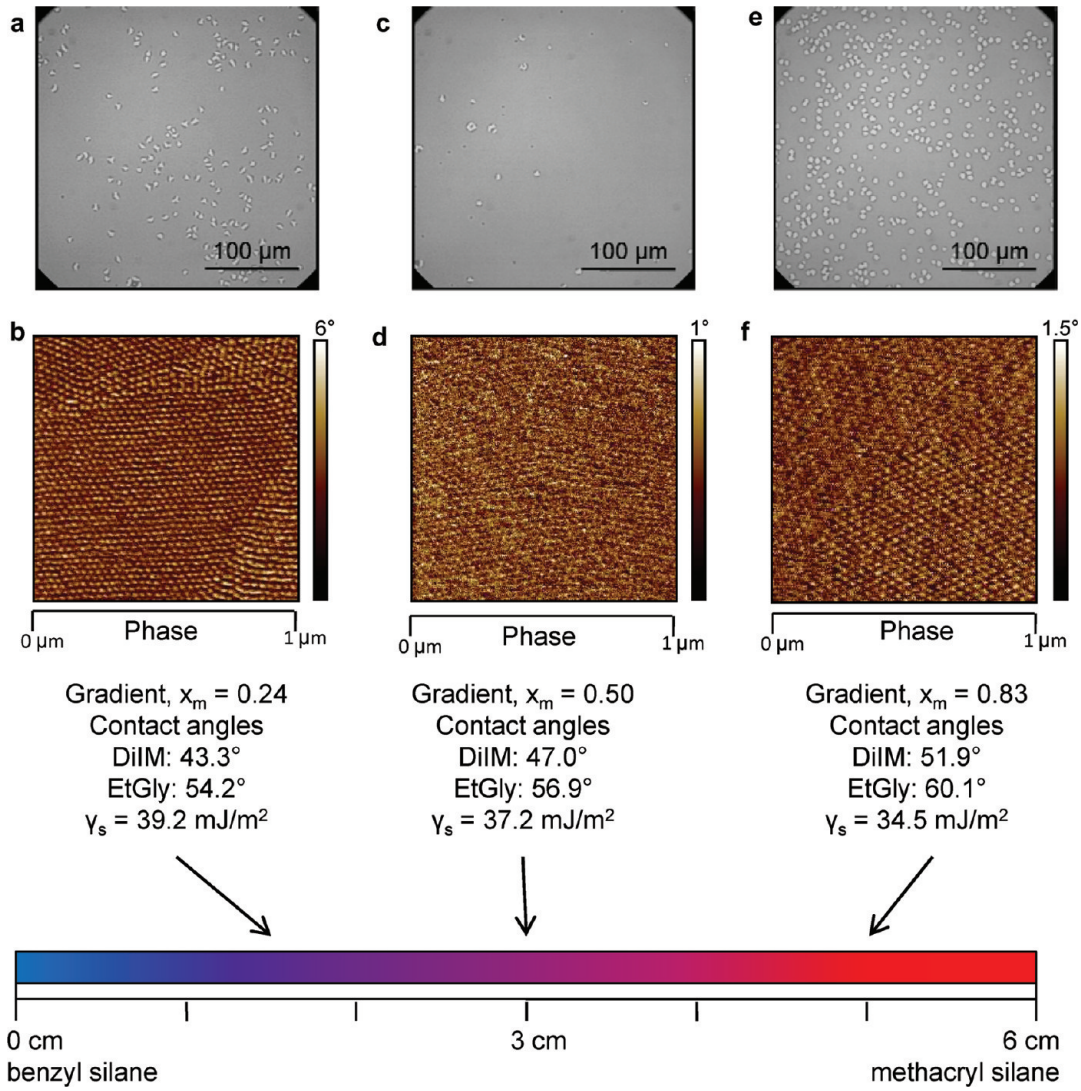

Figure 7. Optical and atomic force microscopy of PS-*b*-PMMA film on gradient monolayer taken at positions 1.5 cm (a,b), 3 cm (c,d), and 5 cm (e,f) from the benzyl silane end of the gradient. Optical micrographs (a,c,e) show a lack of island/hole features across the majority of the film, until position ≈5 cm. AFM phase images reveal perpendicular and parallel microstructure orientations corresponding to the lack of, or presence of, islands/holes, respectively. The composition (x_m), the diiodomethane (DiIm) and ethylene glycol (EtGly) contact angles, and the surface energy (γ_s) at each position are provided for reference.

above equation correlate well with the compositions determined experimentally from XPS, following the expected $y = x$ trend line with an $r^2 \approx 0.99$ (Figure 5b). Thus, we validate the use of diiodomethane contact angle as an estimator of composition for this two-component system.

Block Copolymer Thin Film Study. Uniform thickness thin films of a cylinder-forming PS-*b*-PMMA block copolymer were flow coated on the fabricated pure component and gradient monolayer substrates. The thickness of all films was ≈70 nm, as measured by interferometry (≈2.9 × L_0, where L_0 is the bulk domain spacing). Films were annealed under vacuum at 170 °C for 24 h and then imaged with optical and atomic force microscopy (AFM).

On UVO-cleaned silicon with native oxide, we observe island/hole formation, indicative of parallel structures. Island/hole formation is identified by optical microscopy (Figure 6a) and verified by AFM height imaging and sections (Figure 6b,c). The parallel microstructure is clear from AFM phase imaging (Figure 6d). Since the native oxide is preferential for the PMMA block, the island/hole formation and parallel microstructure are expected.

On the pure monolayer samples, we also observe island/hole formation and parallel microstructures (Figure 6e−h and i−l). These structures are expected because the benzyl silane should be preferential for the PS block and the methacryl silane should be preferential for the PMMA block.

We examined three points along the gradient sample and found that a wide range of monolayer compositions produced a relatively neutral surface, as indicated by a transition from island/hole structures to featureless film in the optical micrographs and

perpendicularly oriented microstructures observed in the AFM phase images. At a position 1.5 cm from the benzyl silane end of the gradient ($x_m = 0.24$, $\gamma_s = 39.2$ mJ/m^2), we observed some areas containing island/hole structures but also far more featureless regions (Figure 7a). AFM phase imaging shows that the microstructure is primarily oriented perpendicular to the substrate (Figure 7b). At a position 3 cm from the benzyl silane end of the gradient ($x_m = 0.50$, $\gamma_s = 37.2$ mJ/m^2), the optical micrograph shows very few island/hole features (Figure 7c) and AFM phase imaging reveals perpendicular structure (Figure 7d). At a position 5 cm from the benzyl silane end of the gradient ($x_m = 0.83$, $\gamma_s = 34.5$ mJ/m^2), the density of island/hole features increases in the optical micrograph (Figure 7e) and AFM phase imaging indicates a mix of regions with perpendicular microstructure and regions that appear to be transitioning from perpendicular to parallel microstructure (Figure 7f).

Having established the utility of this surface energy/chemistry gradient to produce the expected morphological changes in a cylinder-forming PS-*b*-PMMA thin film, our method can be readily applied to mapping the phase behavior of PS-*b*-PMMA block copolymers of differing molecular weights, compositions, and morphologies and to generating gradients with different chemical functionalities to investigate the thin film phase behavior of other block copolymer systems.

CONCLUSIONS

We have presented a single-step, vapor deposition method for generating two-component gradients with linear surface energy and composition profiles. For the given two-component system, the gradient profiles were easily tuned by manipulating reservoir size and position. Additionally, the characteristics of the gradient were independent of time as long as maximum coverage of the surface was achieved. We created a gradient with chemical functionalities that mimic the structures of PS and PMMA and demonstrated the utility of the fabricated gradient in a PS-*b*-PMMA thin film morphology study in which we identified the expected morphological changes across the gradient.

By changing the functionalities of the chlorosilane materials used, our controlled vapor deposition method can be used to create gradient surfaces with a wide range of surface chemistries and surface energies. Given the versatility and facile implementation of our method, we envision numerous applications including the investigation of surface energy/chemistry effects on block copolymer thin film self-assembly, both for PS-*b*-PMMA and for other copolymer systems, studies of wettability and adhesion, and deposition of chemically reactive moieties that enable additional surface chemistry/functionalization. We anticipate the use of our gradient method for the development of nanotechnologies in the chemical, physical, and biological sciences.

METHODS

Materials. Benzyldimethylchlorosilane (CAS 1833-31-4) [benzyl silane] and 3-methacryloxypropyldimethylchlorosilane (CAS 24636-31-5) [methacryl silane] were obtained from Gelest, Inc. and used as received.[30] Toluene was argon-purged and further purified by passage through a neutral alumina column and a Q5 catalyst column before use. Silicon wafers (N⟨100⟩, Wafer World, Inc.) were rinsed with toluene, placed in a UVO cleaner (model 342, Jelight Co., Inc.) for 1 h, then re-rinsed with toluene prior to use. Deionized (DI) water for contact angle measurements was purified with a Milli-Q reagent water purification system. Diiodomethane (99+%, stabilized, Acros Organics) was used as received. Ethylene glycol (99.5%, analysis grade, Acros Organics) was dried by vacuum distillation over sodium hydroxide (certified ACS grade, Fisher Scientific) and stored on molecular sieves (Type 4A, 8-12 mesh beads, grade S14, Fisher Scientific) in a desiccator under vacuum. Poly(styrene-*b*-methyl methacrylate) (PS-*b*-PMMA) was obtained from Polymer Source, Inc. and had a number average relative molecular mass of $M_n = 47\,700$ g/mol ($M_w/M_n = 1.04$) and a PS volume fraction of $f_{PS} = 0.77$ (calculated using homopolymer densities at 140 °C).[31] The bulk morphology was hexagonally packed cylinders with a domain spacing of 24 nm as characterized by small-angle X-ray scattering and transmission electron microscopy.

Contact Angle. Water, diiodomethane, and ethylene glycol static contact angles were measured using a First Ten Ångstroms (FTÅ) 125 contact angle measuring system. Liquid drops (2 μL) were dispensed and placed on the surface with a Distriman pipet. Angle analysis was performed using FTÅ software and the drop shape method applied after the drop shape had stopped changing (0.1 s for water, 0.3 s for diiodomethane, and 0.8 s for ethylene glycol). Thus, equilibrium contact angles were obtained for use in surface energy calculations. Reported contact angles were averaged over multiple spots from multiple samples; error bars represent one standard deviation of the data from repeated measurements, which is taken as the experimental uncertainty of the measurement.

Surface energies were calculated using the Owens−Wendt method,[28] an extension of the Good−Girifalco geometric mean approximation method.[32] Using the combining rule supplied by this method, the following set of equations was solved simultaneously:

$$(1 + \cos(\theta))\gamma_{L,DiIM} = 2(\sqrt{\gamma_S^D}\gamma_{L,DiIM}^D + \sqrt{\gamma_S^P}\gamma_{L,DiIM}^P)$$

$$(1 + \cos(\theta))\gamma_{L,EtGly} = 2(\sqrt{\gamma_S^D}\gamma_{L,EtGly}^D + \sqrt{\gamma_S^P}\gamma_{L,EtGly}^P)$$

where γ_L is the liquid surface tension, with dispersive components γ_L^D and polar components γ_L^P, for diiodomethane (DiIM) or ethylene glycol (EtGly), and γ_S is the surface energy, with dispersive component γ_S^D and polar component γ_S^P. The liquid surface tensions (mN/m) used in these calculations were $\gamma_{L,DiIM} = 50.8$, $\gamma_{L,DiIM}^D = 50.8$, $\gamma_{L,DiIM}^P = 0$, $\gamma_{L,EtGly} = 48.0$, $\gamma_{L,EtGly}^D = 29.0$, $\gamma_{L,EtGly}^P = 19.0$.

X-ray Photoelectron Spectroscopy (XPS). XPS measurements were carried out at the National Institute of Standards and Technology on a Kratos AXIS Ultra DLD spectrometer at a vacuum of 8×10^{-9} Torr with a monochromatic Al source and power of 140 W. Survey spectra were collected over a binding energy range from 1100 to 0 eV with a step size of 0.5 eV using a pass energy of 160 eV and a 100 ms dwell time. High-resolution scans (O 1s, C

1s, and Si 2p) were collected using a step size of 0.1 eV and a pass energy of 20 eV. Sweep times and number of sweeps were 60 s × 3 sweeps (O 1s), 120 s × 10 sweeps (C 1s), and 60 s × 3 sweeps (Si 2p). A charge neutralizer was operated at a filament current of 1 A and a charge balance of 1.5 V to prevent sample charging. We sampled four points on each pure component monolayer and 13 points along the gradient monolayer. Binding energies were calibrated with respect to C 1s at 285.0 eV. After subtraction of a Shirley baseline, all spectra were fitted using 70% Gaussian/30% Lorentzian peaks. The fitting parameters were peak position, full width at half-maximum, and intensity. Initial estimates for binding energy peak locations were based on homopolymer spectra found in the literature.[33] The four C 1s curve fits for each of the pure component monolayers were averaged to generate the final pure component monolayer curves used to fit gradient monolayer spectra. The gradient C 1s spectra were fit as linear combinations of the pure component monolayer curves; the error associated with each fit was calculated by

$$\frac{\int (y - \hat{y})dx}{\int y dx}$$

where $y - \hat{y}$ is the residual and y is the intensity at each binding energy, x.

Polymer Film Preparation. Uniform thickness PS-*b*-PMMA films were cast on the modified substrates by flow coating[34] from a 3 mass % solution of polymer dissolved in toluene. Our films were flow coated with 50 μL of solution, a gap height of 200 μm, and a velocity of 11 mm/s to achieve a desired film thickness of ≈70 nm. Film thickness measurements were obtained using a Filmetrics F20-UV interferometer operated in reflectance mode. The films were dried under vacuum by slowly increasing the temperature up to 80 °C and holding at 80 °C for 15 h prior to high-temperature annealing at 170 °C for 24 h.

Optical and Atomic Force Microscopy (AFM). Optical microscopy images were collected on a microscope equipped with a CCD camera at 50× magnification. Tapping mode AFM images were collected using a Veeco Dimension 3100 atomic force microscope with a Nanoscope IV control unit. Silicon probes (Nanosensors) with a resonant frequency between 146 and 236 kHz and a force constant between 21 and 98 N/m were used to image the polymer films.

Acknowledgment. This work was supported by the National Science Foundation through DMR-0645586 and a National Science Foundation Graduate Research Fellowship to J.N.L.A. We thank T. Beebe, Jr., Department of Chemistry, University of Delaware, for use of his contact angle measuring system and the National Institute of Standards and Technology for the use of their XPS facility. This paper is an official contribution of the National Institute of Standards and Technology.

Supporting Information Available: Survey, high-resolution oxygen 1s (O 1s) and silicon 2p (Si 2p) spectra for pure component monolayers. High-resolution carbon 1s (C 1s) spectra for points sampled on the gradient monolayer. This material is available free of charge *via* the Internet at http://pubs.acs.org.

REFERENCES AND NOTES

1. Genzer, J.; Bhat, R. R. Surface-Bound Soft Matter Gradients. *Langmuir* **2008**, *24*, 2294–2317.
2. Smith, A. P.; Sehgal, A.; Douglas, J. F.; Karim, A.; Amis, E. J. Combinatorial Mapping of Surface Energy Effects on Diblock Copolymer Thin Film Ordering. *Macromol. Rapid Commun.* **2003**, *24*, 131–135.
3. Genzer, J.; Kramer, E. J. Wetting of Substrates with Phase-Separated Binary Polymer Mixtures. *Phys. Rev. Lett.* **1997**, *78*, 4946–4949.
4. Ashley, K. M.; Raghavan, D.; Douglas, J. F.; Karim, A. Wetting-Dewetting Transition Line in Thin Polymer Films. *Langmuir* **2005**, *21*, 9518–9523.
5. Epps, T. H.; DeLongchamp, D. M.; Fasolka, M. J.; Fischer, D. A.; Jablonski, E. L. Substrate Surface Energy Dependent Morphology and Dewetting in an ABC Triblock Copolymer Film. *Langmuir* **2007**, *23*, 3355–3362.
6. Mansky, P.; Liu, Y.; Huang, E.; Russell, T. P.; Hawker, C. Controlling Polymer−Surface Interactions with Random Copolymer Brushes. *Science* **1997**, *275*, 1458–1460.
7. Ham, S.; Shin, C.; Kim, E.; Ryu, D. Y.; Jeong, U.; Russell, T. P.; Hawker, C. J. Microdomain Orientation of PS-*b*-PMMA by Controlled Interfacial Interactions. *Macromolecules* **2008**, *41*, 6431–6437.
8. Han, E.; Stuen, K. O.; La, Y.-H.; Nealey, P. F.; Gopalan, P. Effect of Composition of Substrate-Modifying Random Copolymers on the Orientation of Symmetric and Asymmetric Diblock Copolymer Domains. *Macromolecules* **2008**, *41*, 9090–9097.
9. Elwing, H.; Welin, S.; Askendal, A.; Nilsson, U.; Lundstrom, I. A Wettability Gradient Method for Studies of Macromolecular Interactions at the Liquid/Solid Interface. *J. Colloid Interface Sci.* **1987**, *119*, 203–210.
10. Chaudhury, M. K.; Whitesides, G. M. How to Make Water Run Uphill. *Science* **1992**, *256*, 1539–1541.
11. Chang, T.; Rozkiewicz, D. I.; Ravoo, B. J.; Meijer, E. W.; Reinhoudt, D. N. Directional Movement of Dendritic Macromolecules on Gradient Surfaces. *Nano Lett.* **2007**, *7*, 978–980.
12. Daniel, S.; Chaudhury, M. K.; Chen, J. C. Fast Drop Movements Resulting from the Phase Change on a Gradient Surface. *Science* **2001**, *291*, 633–636.
13. Daniel, S.; Sircar, S.; Gliem, J.; Chaudhury, M. K. Ratcheting Motion of Liquid Drops on Gradient Surfaces. *Langmuir* **2004**, *20*, 4085–4092.
14. Genzer, J.; Efimenko, K.; Fischer, D. A. Formation Mechanisms and Properties of Semifluorinated Molecular Gradients on Silica Surfaces. *Langmuir* **2006**, *22*, 8532–8541.
15. Choi, S.-H.; Newby, B. Z. Micrometer-Scaled Gradient Surfaces Generated Using Contact Printing of Octadecyltrichlorosilane. *Langmuir* **2003**, *19*, 7427–7435.
16. Kraus, T.; Stutz, R.; Balmer, T. E.; Schmid, H.; Malaquin, L.; Spencer, N. D.; Wolf, H. Printing Chemical Gradients. *Langmuir* **2005**, *21*, 7796–7804.
17. Morgenthaler, S.; Lee, S.; Zurcher, S.; Spencer, N. D. A Simple, Reproducible Approach to the Preparation of Surface-Chemical Gradients. *Langmuir* **2003**, *19*, 10459–10462.
18. Berry, B. C.; Stafford, C. M.; Pandya, M.; Lucas, L. A.; Karim, A.; Fasolka, M. J. Versatile Platform for Creating Gradient Combinatorial Libraries *via* Modulated Light Exposure. *Rev. Sci. Instrum.* **2007**, *78*, 072202.
19. Gallant, N. D.; Lavery, K. A.; Amis, E. J.; Becker, M. L. Universal Gradient Substrates for "Click" Biofunctionalization. *Adv. Mater.* **2007**, *19*, 965−−969.
20. Bhat, R.; Sell, S.; Trimbach, D. C.; Zankovych, S.; Zhang, J.; Bossert, J.; Klemm, E.; Jandt, K. D. Multiple Surface Functionalities through Step-by-Step Hydrolysis of Self-Assembled Monolayers. *Chem. Mater.* **2008**, *20*, 5197–5202.
21. Iqbal, P.; Critchley, K.; Attwood, D.; Tunnicliffe, D.; Evans, S. D.; Preece, J. A. Chemical Manipulation by X-rays of Functionalized Thiolate Self-Assembled Monolayers on Au. *Langmuir* **2008**, *24*, 13969–13976.
22. Xu, C.; Barnes, S. E.; Wu, T.; Fischer, D. A.; DeLongchamp, D. M.; Batteas, J. D.; Beers, K. L. Solution and Surface Composition Gradients *via* Microfluidic Confinement: Fabrication of a Statistical-Copolymer-Brush Composition Gradient. *Adv. Mater.* **2006**, *18*, 1427–1430.
23. Elkasabi, Y.; Lahann, J. Vapor-Based Polymer Gradients. *Macromol. Rapid Commun.* **2009**, *30*, 57–63.
24. Peng, D. K.; Ahmadi, A. A.; Lahann, J. A Synthetic Surface that Undergoes Spatiotemporal Remodeling. *Nano Lett.* **2008**, *8*, 3336–3340.

25. Bain, C. D.; Troughton, E. B.; Tao, Y. T.; Evall, J.; Whitesides, G. M.; Nuzzo, R. G. Formation of Monolayer Films by the Spontaneous Assembly of Organic Thiols from Solution onto Gold. *J. Am. Chem. Soc.* **1989**, *111*, 321–335.
26. Julthongpiput, D.; Fasolka, M. J.; Zhang, W.; Nguyen, T.; Amis, E. J. Gradient Chemical Micropatterns: A Reference Substrate for Surface Nanometrology. *Nano Lett.* **2005**, *5*, 1535–1540.
27. Roskov, K. E.; Epps, T. H.; Berry, B. C.; Hudson, S. D.; Tureau, M. S.; Fasolka, M. J. Preparation of Combinatorial Arrays of Polymer Thin Films for Transmission Electron Microscopy Analysis. *J. Comb. Chem.* **2008**, *10*, 966–973.
28. Owens, D. K.; Wendt, R. C. Estimation of the Surface Free Energy of Polymers. *J. Appl. Polym. Sci.* **1969**, *13*, 1741–1747.
29. Clint, J. H.; Wicks, A. C. Adhesion under Water: Surface Energy Considerations. *Int. J. Adhes. Adhes.* **2001**, *21*, 267–273.
30. Certain commercial materials and equipment are identified in this paper in order to specify adequately the experimental procedure. In no case does such identification imply recommendation by the National Institute of Standards and Technology nor does it imply that the material or equipment identified is necessarily the best available for this purpose.
31. Fetters, L. J.; Lohse, D. J.; Richter, D.; Witten, T. A.; Zirkel, A. Connection between Polymer Molecular Weight, Density, Chain Dimensions, and Melt Viscoelastic Properties. *Macromolecules* **1994**, *27*, 4639–4647.
32. Good, R. J.; Girifalco, L. A. A Theory for Esimation of Surface and Interfacial Energies. III. Esimation of Surface Energies of Solids from Contact Angle Data. *J. Phys. Chem.* **1960**, *64*, 561–565.
33. Beamson, G.; Briggs, D. *High Resolution XPS of Organic Polymers*; John Wiley & Sons Ltd: New York, 1992.
34. Stafford, C. M.; Roskov, K. E.; Epps, T. H.; Fasolka, M. J. Generating Thickness Gradients of Thin Polymer Films *via* Flow Coating. *Rev. Sci. Instrum.* **2006**, *77*, 023908.